Fast ^{18}F Labeling of a Near-Infrared Fluorophore Enables Positron Emission Tomography and Optical Imaging of Sentinel Lymph Nodes

Richard Ting,[†] Todd A. Aguilera,[†] Jessica L. Crisp,[†] David J. Hall,[‡] William C. Eckelman,[‡] David R. Vera,[‡] and Roger Y. Tsien*,[†,§]

Department of Pharmacology 0647, Department of Radiology, and Howard Hughes Medical Institute, University of California, San Diego, La Jolla, California 92093. Received March 11, 2010; Revised Manuscript Received June 24, 2010

We combine a novel boronate trap for F^- with a near-infrared fluorophore into a single molecule. Attachment to targeting ligands enables localization by positron emission tomography (PET) and near-infrared fluorescence (NIRF). Our first application of this generic tag is to label Lymphoseek (tilmanocept), an agent designed for receptor-specific sentinel lymph node (SLN) mapping. The new conjugate incorporates $^{18}F^-$ in a single, aqueous step, targets mouse SLN rapidly (1 h) with reduced distal lymph node accumulation, permits PET or scintigraphic imaging of SLN, and enables NIRF-guided excision and histological verification even after ^{18}F decay. This embodiment is superior to current SLN mapping agents such as nontargeted [^{99m}Tc]sulfur colloids and Isosulfan Blue, as well as the phase III targeted ligand [^{99m}Tc]SPECT Lymphoseek counterpart, species that are visible by SPECT or visible absorbance separately. Facile incorporation of ^{18}F into a NIRF probe should promote many synergistic PET and NIRF combinations.

INTRODUCTION

Different molecular imaging techniques have complementary advantages and disadvantages in spatial and temporal resolution, depth penetration, sensitivity, and cost (*1*). A powerful way to combine synergistic advantages is to construct synthetic probes that can be imaged by two or more modalities (*2*−*4*). Radiotracers and near-infrared fluorescence (NIRF) are particularly suitable combinations because both are sufficiently sensitive to enable direct visualization at receptor binding concentrations (nanomolar to picomolar). In contrast, magnetic resonance imaging (MRI) and X-ray contrast tomography require much higher elemental concentrations of the probe (*1*). The excellent penetration of γ-ray photons in positron emission tomography (PET) allows quantitative detection regardless of depth, making this technique ideal for whole-body scanning. NIRF offers much higher spatial and temporal resolution and cheaper instrumentation, but it is largely limited to superficial targets, making it ideal for image-guided surgery and histology.

Multimodality PET/optical probes under development currently include ^{18}F/quantum dot (QD) (*5*), ^{18}F/nanoparticle (*6*), bis(thiosemicarbazonato) ^{64}Cu chelates (*3, 7*), and ^{64}Cu/cypate (*4*) conjugates. PET bioconjugate radiochemistry is often limited to the physically more common radionuclides ^{64}Cu ($t_{1/2}$ = 762 min), ^{68}Ga ($t_{1/2}$ = 68 min), and ^{18}F ($t_{1/2}$ = 110 min), because they are easily manipulated and possess nuclear half-lives sufficiently long enough for chemical isotope manipulation and in vivo distribution. Unfortunately, each of these PET nuclides presents intrinsic complications. For example, ^{64}Cu (*3, 4, 8*) and ^{68}Ga (*9, 10*) chelates can suffer from impure isotope production as well as lowered specific activity because of impure isotope decay (*11*) and large chelation moieties that may alter ligand biodistribution and may also suffer from in vivo metal ion transchelation (*12*). Alternatively, traditional ^{18}F labeling methods (*5, 13*−*17*) relying on C−F bond formation are water-sensitive, multistep processes that often require harsh reaction conditions and long processing times that are poorly suited to the short half-life of ^{18}F.

To simplify PET chemistry, there has been recent interest in developing rapid, one-step labeling procedures from shelf-stable final target precursors with aqueous $^{18}F^-$, while reducing the side products and chromatographic purifications associated with traditional C−^{18}F labelings. Recent silica-based (*18*−*21*) and boron-based (*22*−*24*) aqueous ^{18}F capture technology allows direct preparation of isotopically pure PET compounds that are cleanly labeled, are easily purified, and have been shown to be stable in vivo (*19, 25*). We chose to generate [^{18}F]fluoroborates because they require less bulky hydrophobic substituents and potentially triple the F^- incorporation stoichiometry and attainable specific activity (*22*−*24*). A typical preparation of ^{18}F fluoride has a specific activity of ∼10 Ci/μmol even if no carrier was deliberately added and therefore contains 170 atoms of ^{19}F for each atom of ^{18}F (*26*). Incorporation of three fluorine atoms triples the probability that at least one will be radioactive. We combine this boron-based ^{18}F capture technology [$t_{1/2}$ of B−F solvolysis = 5550 ± 1740 min (*23*)] with a NIR fluorophore to give a generally conjugatable PET/NIRF multimodality probe **1** (Figure 1A). Our first test of this probe is to help find and excise sentinel lymph nodes.

The current method for sentinel lymph node mapping in melanoma and breast cancer involves injection of a combination of Isosulfan Blue (*27*) and a ^{99m}Tc-labeled colloid radiopharmaceutical (*28, 29*). This pair allows for lymphoscintigraphy and absorbance-guided intraoperative lymph node excision (*30*). With little affinity for the sentinel lymph node, ^{99m}Tc-labeled colloids and Isosulfan Blue will travel past the sentinel node in a lymph chain restricting the surgeon to a small time-window within which to perform the mapping procedure. ^{99m}Tc-radiolabeled colloids are large particles that are nonspecifically trapped within lymphoid tissue. These agents are inefficient at entering lymph channels and, over time, reach distal lymph nodes. Distal colloid or dye uptake leads to the surgical removal of more lymph nodes than necessary, which increases the extent of the dissection, forces the pathologist to review a greater

* To whom correspondence should be addressed.
[†] Department of Pharmacology 0647.
[‡] Department of Radiology.
[§] Howard Hughes Medical Institute.

10.1021/bc1001328
Published on Web 09/27/2010

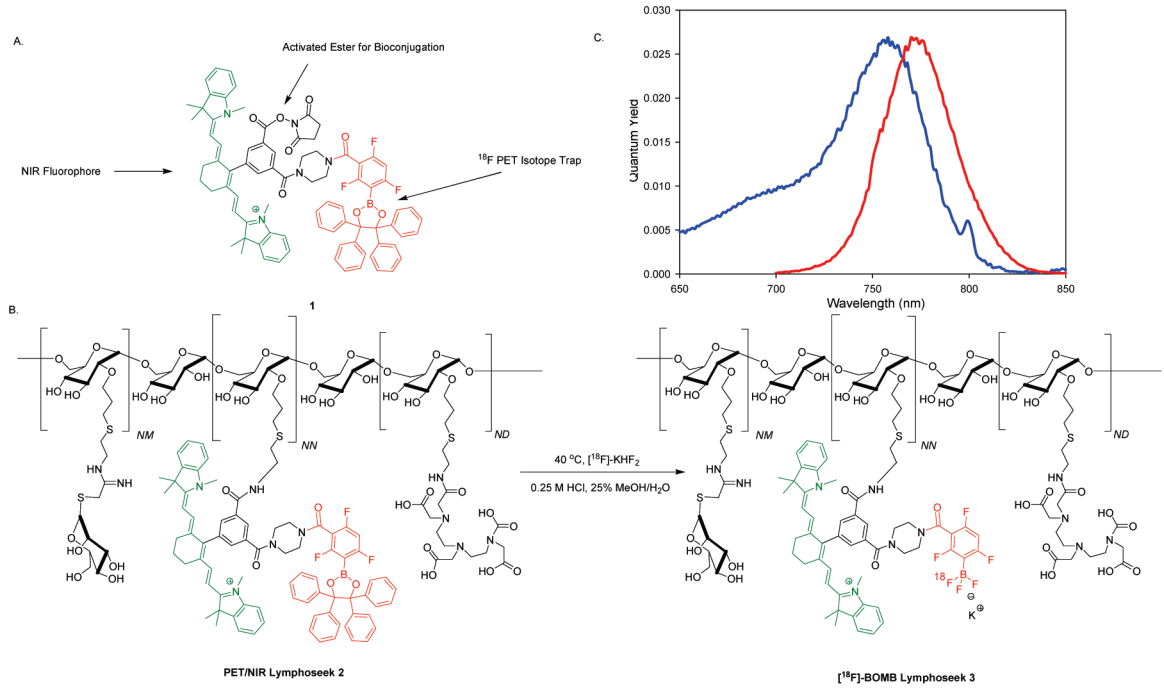

Figure 1. (A) Structure of the ^{18}F boron trap/heptamethine cyanine (C7-Cy) PET/NIR probe, [^{18}F]BOMB **1**, activated as an NHS ester for general bioconjugation. The boron-based ^{18}F trap is colored red, while the NIR fluorophore is colored green. (B) Structure of PET/NIR dual probe Lymphoseek (DTPA-mannosyl-dextran) **2** and the aqueous ^{18}F labeling scheme used to generate ^{18}F-labeled [^{18}F]BOMB Lymphoseek **3**. (C) Excitation (blue) and emission (red) spectra of an aqueous solution of [^{18}F]PET/NIR-Lymphoseek **3** ($\varphi_f = 0.027$, excitation maximum = 755 nm, emission maximum = 772 nm, 1.5 μM Lymphoseek solution in water). The amine (NN), mannose (NM), and DTPA (ND) densities on Lymphoseek are 5.8, 16.5, and 4.2 mol/dextran, respectively. The average preconjugation molecular weight of Lymphoseek is 16122.

number of lymph nodes, and increases the probability of local lymphedema, a complication of lymph node resection. An alternative probe is Lymphoseek (tilmanocept), a mannosylated 16 kDa dextran conjugate, that can be labeled with ^{99m}Tc for SPECT-based imaging (*31, 32*) and is currently in phase III clinical trials. It binds with a high affinity to cell-surface lectins [$K_D = 0.12$ nM (*33*)] and was developed specifically for sentinel lymph node mapping. ^{99m}Tc-labeled Lymphoseek has demonstrated rapid injection site clearance, a low level of distal node accumulation, a lack of local systemic toxicity, and greater specific sentinel lymph node uptake than filtered [^{99m}Tc]sulfur colloid (*32, 34, 35*). A version of Lymphoseek that can be viewed by both PET and NIRF would combine molecular targeting, the higher spatial resolution of PET compared to ^{99m}Tc SPECT, and the greater sensitivity and depth penetration of NIRF compared to the red absorbance of Isosulfan Blue.

Here we apply our generally conjugatable PET/NIRF probe **1** (Figure 1A) to Lymphoseek to enable multimodality-guided sentinel node visualization and excision. This [^{18}F]boron/optical multimodality beacon ([^{18}F]BOMB) is differentiated from traditional C−^{18}F PET labeling strategies (*5, 13*−*17*) by its one-step [^{18}F]fluoride wash-in labeling. [^{18}F]BOMB Lymphoseek **3** (Figure 1B) allows rapid, receptor-specific, positive identification of the sentinel lymph node in both the NIRF and PET imaging modes while maintaining little breakthrough to distal lymph nodes. This success predicts that [^{18}F]BOMB should be generalizable to other medically relevant targets.

EXPERIMENTAL PROCEDURES

Chemical Synthesis. *PET/NIR Dual-Probe Reaction with Lymphoseek: Synthesis of PET/NIR Lymphoseek Probe* ***2.*** The generally conjugatable NHS ester of PET/NIR probe **1** (4 μmol) (see the Supporting Information for detailed synthesis) was added as a CH_2Cl_2 solution directly into a 1.5 mL glass vial containing 5.5 mg (0.34 μmol) of Lymphoseek bearing 5.8 amine groups per dextran (Reliable Biopharmaceuticals). This solution was concentrated to dryness and then resuspended in 100 μL of DMF. This solution was sonicated for 1 h and left to react for 18 h. The next day, 10 μL of diisopropylethylamine was added and the reaction mixture was left for an additional 2 h. The reaction mixture was then transferred to a polypropylene centrifuge tube containing 25 mL of CH_2Cl_2. A pellet of **2** was isolated following centrifugation for 20 min at 3000 rcf, washed with two more portions of CH_2Cl_2, dried under high vacuum, and resuspended in 1 mL of water. This solution was centrifuged for 2 min at 18000 rcf. Water-soluble **2** was decanted from the pellet and divided into four aliquots, which were lyophilized and stored at −78 °C. On the basis of fluorescence readings, 115.9 nmol of fluorophore-conjugated Lymphoseek **2** was isolated. On the basis of a hexose assay (*36*), 34−49 nmol of Lymphoseek was isolated as **2**. This corresponds to a 10−14% yield of **2** from unconjugated Lymphoseek. The incorporation ratio of fluorophore to Lymphoseek was 2.36 to 3.41 fluorophores per molecule of Lymphoseek. Spectrophotometric constants of a 1.5 μM solution in water were as follows: absorbance maximum = 758 nm, $\varepsilon_{758} = 110000$ cm^{-1} M^{-1} per fluorophore, excitation maximum = 757 nm, emission maximum = 777 nm, and quantum yield = 0.026.

Radiochemistry. *^{18}F-Labeled Lymphoseek* ***3.*** A 300−500 μL aqueous solution containing 100 mCi of $^{18}F^-$ was transferred via syringe to a 10 mL glass vial containing 0.4 μL of 0.05 M KHF_2 (40 nmol) fluoride carrier. Note that acidic solutions of $H^{18}F$ are volatile and radioactive, and therefore, the following procedures should be performed in a vented hot cell or a fume hood with radiation shielding. This sample was heated to dryness at 140 °C under a nitrogen flow. The clear dry solid was resuspended in 5 μL of a 0.25 M HCl/25% MeOH/75% H_2O solution. This solution, containing 30 mCi, was transferred to a 600 μL microcentrifuge tube containing 10.6 nmol of lyophilized **2**. This volume was sufficient to completely solubilize **3** and was reacted at 40 °C for 1 h. Following reaction,

the reaction was quenched with 40 μL of a 1 M MOPS buffered solution (pH 7.3).

To remove unreacted [^{18}F]fluoride, 5 μL of 3.0 M KHF_2 was added, and then the entire 45 μL was transferred to a Micro Bio Spin 6 column [molecular weight cutoff of 6000 (Bio-Rad)] buffered with 10 mM Tris (pH 7.4) and centrifuged without added eluant for 4 min at 1000 rcf. To the 40 μL of eluant was added an additional 5 μL of 3.0 M KHF_2 (30 μmol) to prevent the nonspecific elution of [^{18}F]fluoride, and the solution was immediately centrifuged. This described spin column purification was repeated three more times with a fresh spin column each time. Bio-Rad P-6 columns quantitatively remove small MW organic molecule impurities (see the Supporting Information) and 93% of [^{18}F]fluoride per column (99.998% of all [^{18}F]fluoride over four columns). Chromatography took 30 min total, and the final pH of the 60 μL of Tris-buffered, eluted solution was 7−8. Fluorescence showed that 6.0 nmol of ^{18}F-labeled PET/NIRF Lymphoseek **3** was eluted from the spin columns 90 min following $^{18}F^-$ concentration. The volume was 60 μL, and the activity was 300 μCi [total preparation time (reaction and purification) of 90 min]. See the Supporting Information for final analyses.

This purified solution was divided into two 30 μL portions, each sufficient for 3 × 10 μL, 1.0 nmol injections of Lymphoseek. To one portion was added 1.0 μL of a 31 mM solution of unconjugated Lymphoseek to give enough injectate for 3 × 10 μL, 11.0 nmol injections. Injections with specific activities of 0.05 Ci/μmol for 1 nmol Lymphoseek injections and 0.005 Ci/μmol for 11 nmol Lymphoseek injections were conducted for 15−75 min following synthesis and purification (see the Supporting Information for specifics).

*^{19}F (nonradioactive) Labeling of Lymphoseek **3**.* A 10.6 nmol quantity of lyophilized **2** was dissolved in a 0.25 M HCl/25% MeOH/75% H_2O solution in a 600 μL Eppendorf tube and left to react at 40 °C for 1 h. This reaction was quenched and the solution chromatographed under conditions similar to those described above for ^{18}F labeling. Spectrophotometric constants of a 1.5 μM solution of [^{19}F]**3** in water were as follows: absorbance maximum = 756 nm, ε_{756} = 110000 cm^{-1} M^{-1} per fluorophore, excitation maximum = 755 nm, emission maximum = 772 nm, and quantum yield = 0.027 (see the Supporting Information for HPLC characterization).

In Vivo Experiments. The in vivo procedures in this study have all been approved by the University of California, San Diego, Institutional Animal Care and Use Committee. A single subcutaneous injection of **3** was made into the right rear footpad of 20−25 g, 6−8-week-old athymic nude mice (Charles River Laboratories). These mice were anesthetized 20 min prior to injection with isoflurane, taped to black cardboard, and placed in pairs on an imaging stage. Six pairs of injections were made. The injected mice received either a 1 nmol dose or a 11 nmol dose (10 μL each) of 10 mM Tris-buffered [^{18}F]Lymphoseek **3** (pH 7.3). The distribution of [^{19}F]Lymphoseek **3** proceeded for 1 h and 20 min before the mice were euthanized by isoflurane overdose followed by cervical dislocation.

Imaging. PET and CT scanning were conducted on a eXplore Vista PET scanner or eXplore Locus CT scanner from GE Healthcare. PET acquisition was conducted in a single block in static emission mode with a 100−700 keV energy window. All PET scans were 20 min unless specified otherwise. Acquisition and OSEM PET reconstruction were performed with GE Explore Vista 3.1/MMKS Image Software. This reconstructed image was fused with computed tomography (CT) images processed with GE Medical Systems eXplore Utilities. CT Image acquisition was performed at 93 μm resolution over 10 min. PET/CT image fusion was conducted with the open source program amide 0.9.1.

NIRF imaging was conducted using multiple cameras because of radioactive licensing regulations. IR image acquisition of the nonradioactive compositions in Figure 2 was performed on a Maestro small animal imaging instrument (CRI Inc.) with a 820 nm emission filter and a 710−760 nm excitation wavelength. Data were collected over a 0.5−20 s exposure. Image processing was performed with Maestro version 2.0.2 and Photoshop. The Maestro, used for Figure 2, was the best instrument for real-time, fluorescence-guided node excision, although a custom system optimized for real-time intraoperative imaging would be yet more convenient. The success of sentinel lymph node excision was 100% as determined by histology with the Maestro. Because animals containing ^{18}F could not be transported to the Maestro, NIRF in vivo image acquisition of ^{18}F-labeled compounds was performed on two systems closer to the hot cell and PET scanner. The first was an eXplore Optix (ART, Advanced Research Technologies Inc.) optical imaging system. This is a point source-detector system with a 750 nm excitation laser and a 780 nm long pass filter placed before the photomultiplier tube for single-photon fluorescence detection. The regions of interest were raster-scanned in 1.5 mm steps with laser powers ranging from 200 to 800 μW and signal integration times ranging from 200 to 1000 ms per point. Image processing was performed with Optix version 2 and Photoshop. However, the slow raster scan of the Optix made real-time, image-guided node excision difficult, so a custom full field system (*37*) was employed for faster NIRF imaging of ^{18}F-labeled compounds (Figure 3C). This system used a pulsed laser tuned to 720 nm (Mai TaiSpectraPhysics) whose output was passed through an expansion lens and diffuser for uniform area illumination. Area detection of the fluorescence intensity was acquired in reflection mode using a 780 nm fluorescence filter and standard 50 mm lens (Nikon) mounted to a microchannel plate (Picostar HRI, La Vision) for signal amplification, which was coupled to an electron-multiplying CCD camera (Andor) to capture the image. Subsequent image processing was performed with Image J and Photoshop. Both the Optix and custom systems can measure nanosecond decay kinetics to provide extra information about probe lifetime and depth, but this dimension was not exploited here.

Lymph Node Removal and Dissection. Animals were euthanized by isoflurane overdose or CO_2 inhalation followed by cervical dislocation. After the skin had been removed, fluorescent images were taken to improve the visualization of the positions of the fluorescent lymph nodes. With mice placed in prone positions, both right and left sets of lymph nodes were surgically removed in the following order: the left popliteal, the left lumbar, the right lumbar, and the right popliteal. Following excision, nodes were weighted, submersed in Optimal Cutting Temperature (OCT) Compound (Sakura Tissue-Tec # 4585) cryogenic embedding medium, and replaced next to their mouse of origin within the field of view, approximately half a centimeter below the surgical site in the corresponding mouse. In some instances where sentinel node excision was difficult, fluorescence guidance was utilized to guide surgical removal.

Following imaging, samples of blood (vena cava), liver, kidney, spleen, the hind feet (right and left), bone (contralateral femur), and muscle from the contralateral femur were collected.

Histology. Immediately following excision, lymph nodes were weighed and then coated in OCT Compound to prevent lymph nodes from becoming dehydrated during PET/CT/NIRF analysis and overnight scintillation counting. Lymph nodes were frozen at −80 °C for extended periods of time in this preservative. Frozen sections (10 μm) of the lymph nodes were imaged under NIRF conditions on a stereomicroscope (Zeiss, Lumar). Tissue was stained with hematoxylin and eosin and subsequently imaged via light microscopy (Zeiss, Axiovert). Images were

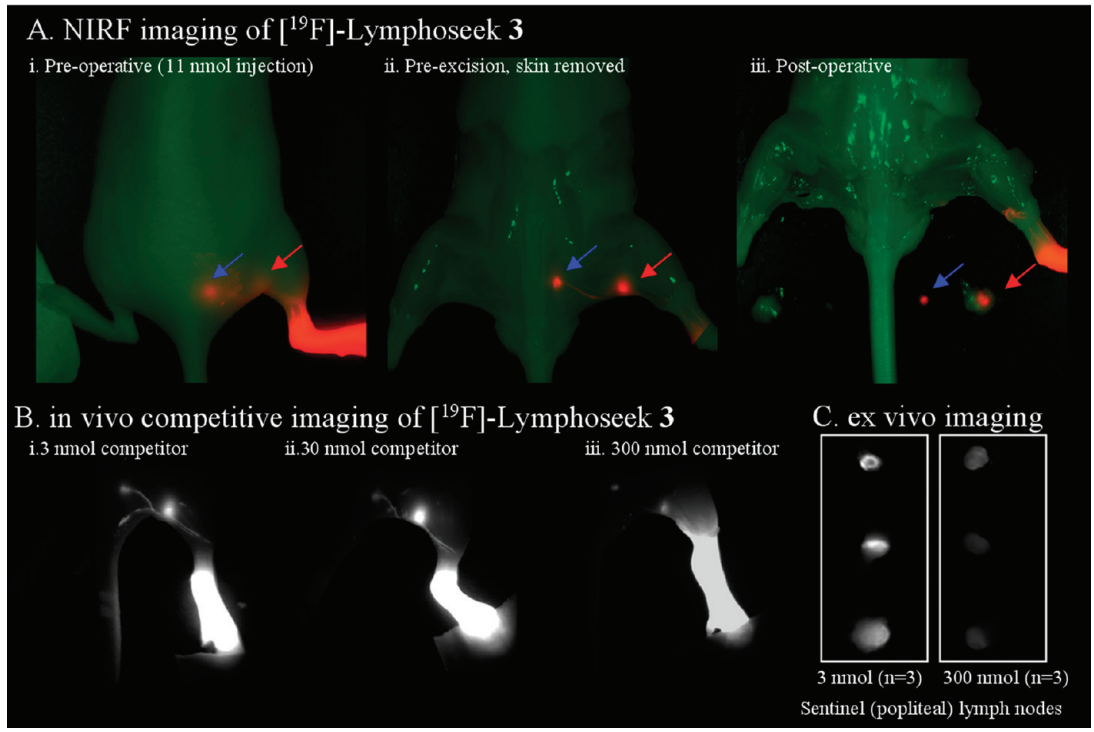

Figure 2. Nonradioactive NIRF imaging of [^{19}F]Lymphoseek **3**. (A) Typical NIRF imaging experiment of a mouse that had been injected with 1 nmol of [^{19}F]**3** diluted with 10 nmol of unconjugated Lymphoseek. The NIRF signal (colored red) is overlaid onto a bright field image (green) of a mouse. A red arrow indicates clear localization of [^{19}F]Lymphoseek **3** to the sentinel (popliteal) lymph node, while the blue arrow indicates localization to the distal (lumbar) lymph node. (i) Post-mortem skin-on image in which tissue (skin) notably interferes with the sentinel lymph node visibility. (ii) Pre-excision image (skin removed) in which the sentinel node visibility is improved and lymph drainage tracks are visible. (iii) Postoperative image in which the excised lymph nodes have been placed in the field of view. (B) In vivo imaging of [^{19}F]Lymphoseek **3**'s mannose receptor specific activity. Fluorescent [^{19}F]Lymphoseek **3** (1 nmol) was imaged in the presence of 2 (i), 29 (ii), or 300 nmol (iii) of unlabeled Lymphoseek, a competitor for lymph node mannose binding sites. Note that lymph tracks are clearly visible and that greater accumulation of fluorescent [^{19}F]Lymphoseek **3** is seen in the sentinel lymph nodes with 3 and 30 nmol injections than with 300 nmol injections because of increased competition with unlabeled Lymphoseek for sentinel lymph node mannose receptors. (C) Ex vivo imaging of [^{19}F]Lymphoseek **3**'s mannose receptor specific activity. Sentinel lymph nodes were extracted from mice and placed on a bed for analysis. Greater accumulation of fluorescent [^{19}F]Lymphoseek **3** is seen in the sentinel lymph nodes in 3 nmol injections than in 300 nmol injections (signal ratio of 3.5, $n = 3$ mice per dose, $P = 0.015$ for a two-tailed test, two-sample equal variance, quantization shown in the Supporting Information).

processed using Image J. The fluorescent histology was acquired using 710/75 nm band-pass excitation and 810/90 nm band-pass emission filters.

Biodistributions. Tissue and injectate samples of known dilutions were assayed (Gamma 9000, Beckman Instruments) for radioactivity using a 400−600 keV energy collection window.

Nonradioactive [^{19}F]Lymphoseek 3 Dosing Experiments. Nonradioactive [^{19}F]Lymphoseek **3** was prepared as described for its ^{18}F counterpart. This preparation was divided into 10 μL aliquots of 10 mM Tris (pH 7.3) that contained 1.0 nmol of ^{19}F-labeled Lymphoseek **3** diluted with 2, 10, 29, or 300 nmol of unlabeled Lymphoseek.

RESULTS

Synthesis and Conjugation of a General PET/NIRF NHS Probe. We appended a sufficiently electron withdrawing boronic ester (*23*) to a heptamethine cyanine, a member of a class of small-molecule dyes that possess an established safety record (*38, 39*). Through chemistry pioneered by the Achilefu group (*40*), we modified the inexpensive synthon IR-775 (Sigma-Aldrich) into an *N*-hydroxysuccinimide (NHS)-activated pre-PET/NIRF probe **1** (Figure 1A) in three steps with a final yield of 50.7%. The resulting pre-PET/NIRF probe **1** (Figure 1A) shows long wavelength NIR fluorescence and adequate quantum yield [excitation maximum = 755 nm, emission maximum = 772 nm, and $\varphi_f = 0.027$ (Figure 1C)]. It was conjugated to Lymphoseek in a ratio of two to three molecules of fluorophore per molecule of Lymphoseek to give precursor **2** (Figure 1B). Self-quenching on **2** or **3** was not observed (see the Supporting Information).

Nonradioactive Fluorescence-Based Lymphoseek Dosing. Initial staging experiments were conducted for two purposes: (1) to determine what doses, when injected into the right rear footpad, would rapidly identify the (sentinel) popliteal lymph node and minimize flow-through to distal (lumbar) lymph nodes and (2) to determine if the conjugation of Lymphoseek to the PET/NIRF probe had altered Lymphoseek's desired pharmaceutical properties, especially mannose receptor specificity. These experiments were conducted with nonradioactive [^{19}F]Lymphoseek **3** and fluorescence equipment alone, minimizing the use of radioactivity during initial stages of this project. Lymphoseek boronate **2** (Figure 1B) was converted into fluoroborate **3**, and 1 nmol of this fluorescent material was diluted with 0, 2, 10, 29, or 300 nmol of unconjugated Lymphoseek to give 1, 3, 11, 30, or 301 nmol of total Lymphoseek but identical quantities of fluorophore. These mixtures were injected into mice (three injections per dose, 15 mice total). After 80 min, the first two lymph nodes that drain the rear-footpad injection site could be viewed by NIRF (Figure 2A,B).

In 1, 3, 11, and 30 nmol Lymphoseek injections (Figure 3 and panels Bi, A, and Bii of Figure 2, respectively), a high level of uptake in the sentinel node was observed with limited flow-through to distal lymph nodes. Injections where **3** had been diluted with 300 nmol of unlabeled Lymphoseek gave less

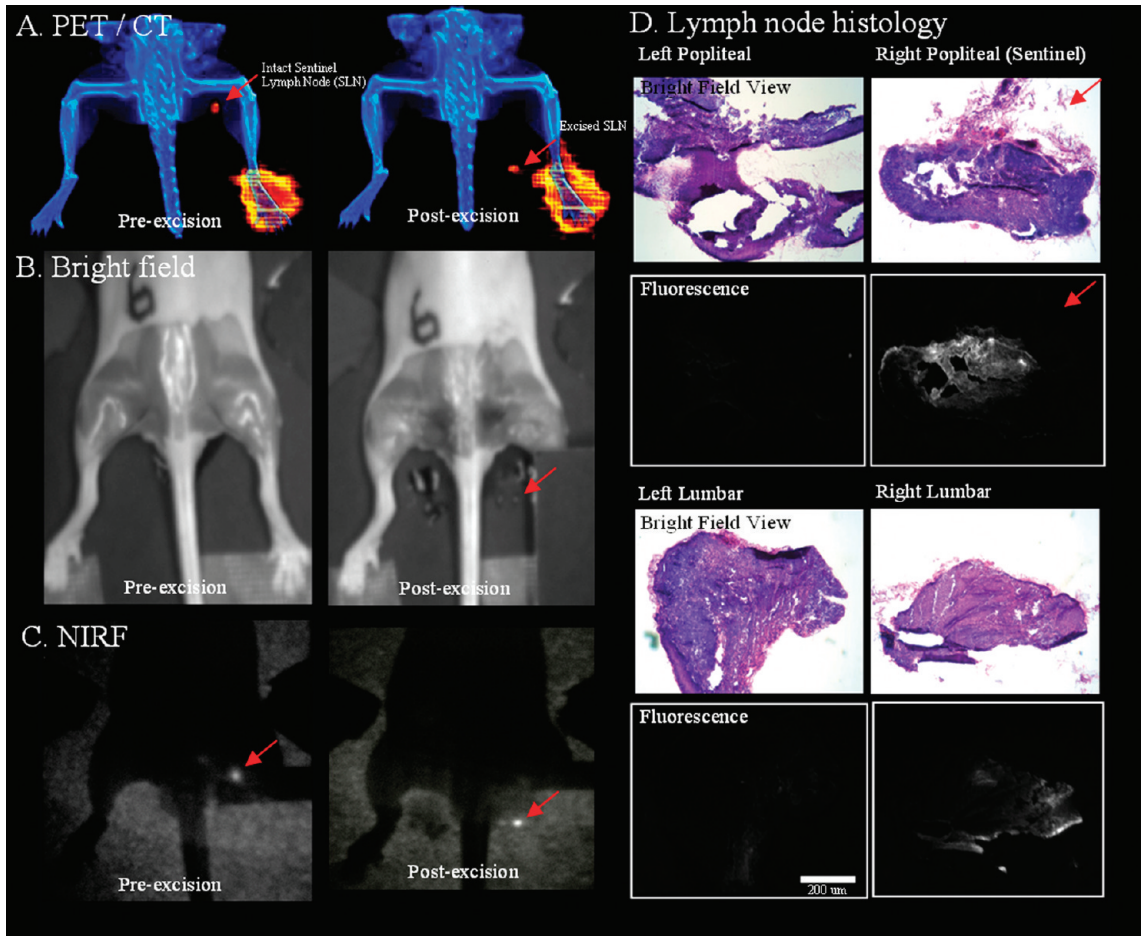

Figure 3. Multimodality imaging of a mouse injected with a 10 μL, 1 nmol, 48.1 μCi dose of ^{18}F-labeled Lymphoseek **3** (0.048 Ci/μmol). The red arrows indicates the location of the sentinel lymph node. (A) Pre-excision, live-mouse PET (red color table)/CT (blue color table) scan (left) and postoperative PET/CT scan (right) of the mouse with excised nodes (right and left lumbar and popliteal) that are placed below the excision site in the field of view. (B) Bright field images of the mouse with skin removed before (left) and after node excision (right). (C) NIRF images taken 90 min postexcision on a custom full field IR camera before (left) and after (right) lymph node excision. The injection site was covered with black cardboard to block intense signal from the foot and allow better visualization of the fluorescent lymph nodes. (D) H and E stain (top, color images) and NIRF (bottom, black and white images) histological verification of lymph node excision. A PET projection video of panel A is given as Supporting Information.

fluorescence in the sentinel lymph node of mice because of competition for SLN mannose receptors (Figure 2Biii,C). Such saturable binding of [^{19}F]Lymphoseek **3** to a limited number of SLN mannose receptors (*32, 34, 41*) suggests that conjugation to **1** does not alter Lymphoseek's mannose receptor specificity. This observation is confirmed quantitatively in separate biodistribution experiments (vide infra).

Image-guided surgical excisions of the SLN were then conducted and confirmed (Figure 2C). Real-time imaging with a NIRF camera allows for rapid and simple removal of lymph nodes, especially because the lymph tracks connecting the nodes are fully visible (Figure 2Bi,Biii). Notably, lymph tracks in mice have not been previously observed with [^{99m}Tc]Lymphoseek. The observed lymph tracks connecting injection sites and nodes should help identify the sentinel node in cases where the distinctions between distal and sentinel nodes are ambiguous.

Radiochemistry. From NIRF experiments (Figure 2), we determined that total doses of Lymphoseek of up to 30 nmol work well in imaging the SLN in mice. Using these doses, we incorporated different ^{18}F activities into **3** to determine the optimal level of radioactivity that would provide sufficient signal to image 1 nmol of Lymphoseek by PET, synthesized on a large multi-injection scale starting with only 100 mCi of $^{18}F^-$ ion. A specific activity of 1−50 Ci/mmol at the time of injection proved to be adequate for imaging ^{18}F-labeled **3** in a 20 min PET scan 1 h after injection.

Size exclusion gel chromatography in spin columns was used to remove small molecule impurities and free [^{18}F]fluoride ions from radiochemical preparations. The removal of [^{18}F]fluoride was evidenced by the absence of a bone signal in PET images (Figure 3A and Supporting Information) (*25*) and biodistribution studies (Figure 4, bone). In mouse serum, the chemical release of F^- from ^{18}F-labeled Lymphoseek **3** had a half-life of 21 h (Supporting Information), 11.6-fold slower than the radioactive decay of ^{18}F.

Multimodality PET/CT/NIRF Imaging. [^{18}F]Lymphoseek **3** was tested for in vivo multimodal imaging in 12 mice. Injections containing 1 nmol and 10−50 μCi of fluorescent **3**, with 0 or 10 nmol of added unlabeled Lymphoseek, were made into the right rear footpad of anesthetized nude mice positioned securely on trays for corroborative multimodality imaging. One hour later, a 20 min PET/CT scan was acquired (Figure 3A, left). Mice were then sacrificed by CO_2 inhalation followed by cervical dislocation; skin was removed, and NIRF images were obtained before (Figure 3C, left) and after excision of nodes, which were placed below their location of origin on the imaging tray. The bright field image of this dissection is shown in Figure 3B (before excision, left, and after excision, right). Successful node excision was confirmed by both NIRF (Figure 3C, right) and PET/CT imaging (Figure 3A, right, and Supporting Information), showing the node signal outside the body. Following image acquisition, tissues were collected for scin-

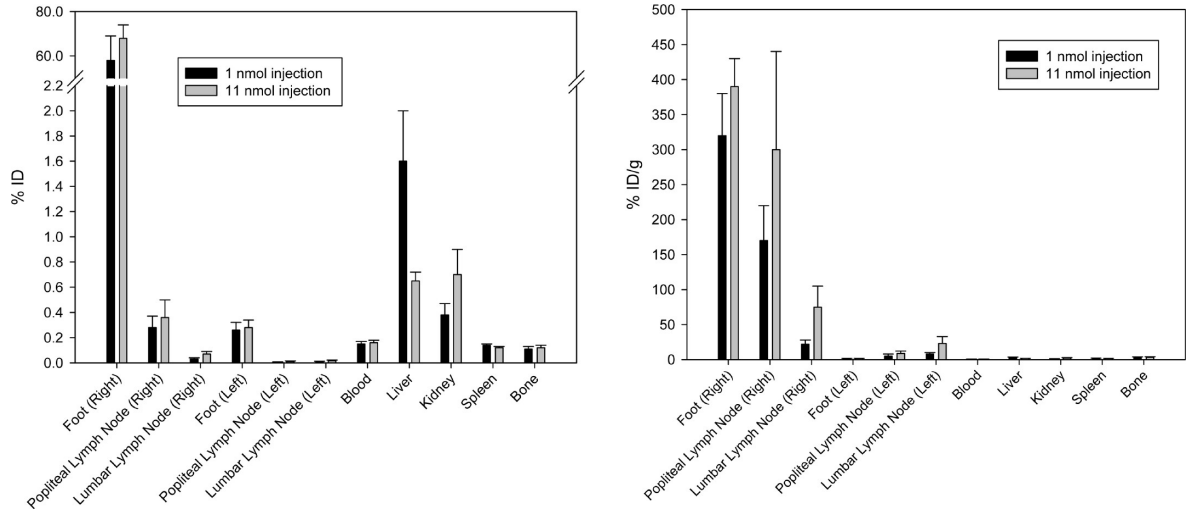

Figure 4. [^{18}F]Lymphoseek **3** tissue biodistribution in mice that were sacrificed 1 h and 20 min following injection. Units of percent injected dose (ID, left) and percent injected dose per gram (right). Biodistribution data from 12 mice were used to compile this figure.

Table 1. Distribution of Radioactive [^{18}F]Lymphoseek 3 in Mice That Were Sacrificed 80 min following Injection[a]

	percent [^{18}F]**3** activity extracted in the sentinel node	Lymphoseek in the sentinel or popliteal lymph node (pmol) (percent of detected nodal Lymphoseek)	Lymphoseek flow-through to the distal or lumbar node (pmol) (percent of detected nodal Lymphoseek)
1 nmol Lymphoseek injection	87 ± 7%	3.0 ± 0.9 (91%)	0.3 ± 0.1 (9%)
11 nmol Lymphoseek injection	74 ± 7%	40 ± 15 (83%)	8 ± 3 (17%)
t test (one-tailed two-sample unequal variance)	$P = 0.022$		$P = 0.033$

[a] Scintigraphy data from six mice were obtained per injected Lymphoseek dose (12 mice total). The percent activity extracted is defined as the difference in counts between the sentinel and distal lymph nodes minus the sum of counts in the sentinel and distal lymph nodes [(counts$_{popliteal}$ − counts$_{lumbar}$)/(counts$_{popliteal}$ + counts$_{lumbar}$)]. The percent of detected nodal Lymphoseek is defined as the amount of Lymphoseek in the lumbar lymph node divided by the sum of the Lymphoseek in both the popliteal and lumbar lymph nodes. Error = $\sigma/(n = 6)^{1/2}$.

tigraphy and histological sectioning (Figure 3D). Little or no flow-through of [^{18}F]Lymphoseek **3** to distal lymph nodes was observed in both NIRF and PET images taken under both injection conditions. PET and NIRF signals were confined to the SLN, the injection site, and, in some cases, the bladder.

Biodistribution. Scintigraphy corroborated the qualitative data observed in PET and IR images (Figure 3A,C). The [^{18}F]Lymphoseek **3** tissue distribution is shown in Figure 4 as the percent of injected dose (% ID) before (left) and after (right) normalization by tissue mass. In 1 and 11 nmol injections of Lymphoseek, the tissues of interest containing the most [^{18}F]Lymphoseek **3** are the right foot (320 ± 60 and 390 ± 40% ID/g per foot, respectively) and the right popliteal (sentinel) lymph node (170 ± 50 and 300 ± 140% ID/g per node, respectively). There is 4−7 times less [^{18}F]Lymphoseek **3** in the ipsilateral distal (lumbar) lymph nodes (22 ± 6 and 75 ± 30% ID/g, respectively) than in the sentinel lymph nodes. Much less [^{18}F]Lymphoseek accumulation is observed in contralateral nodes (5 ± 3 and 9 ± 4% ID/g for contralateral popliteal lymph nodes and 8 ± 2 and 23 ± 10% ID/g for contralateral lumbar lymph nodes, for 1 and 11 nmol injections, respectively). Nonlymphatic tissue, i.e., blood, liver, kidney, spleen, and bone, contained not more than 4% ID/g of [^{18}F]Lymphoseek **3**.

Statistical analysis verified that [^{18}F]Lymphoseek **3** retains receptor targeting properties consistent with [^{99m}Tc]Lymphoseek literature (*32, 41*). In mice treated with 1 nmol of [^{18}F]Lymphoseek, the sentinel node extracted 87 ± 7% (Table 1) of the total lymph node accumulation, significantly greater than 74 ± 7% extracted at an 11 nmol dose. These values correspond to 3 ± 0.9 and 40 ± 15 pmol of total Lymphoseek (3 ± 0.9 and 3.6 ± 1 pmol of ^{18}F-labeled Lymphoseek **3**, respectively) in the sentinel node. These are subsaturating doses of Lymphoseek. The Lymphoseek binding capacity from a rear footpad injection in the popliteal node of mice is 49 ± 25 pmol (*41*).

Histology. NIRF histology (Figure 3D) showed that Lymphoseek **3** indeed localized to SLNs (Figure 3D), though ^{18}F activity was no longer measurable. On the basis of the specific activity of radiolabeling, the majority (>99%) of the fluorescent material was nonradioactive [^{19}F]**3** even before the ^{18}F had decayed. Hematoxylin and eosin (H and E) frozen sections of the excised lymph nodes of mice were prepared and analyzed. Specifically, lymph nodes were confirmed through the observation of an encapsulated dense mass of densely packed lymphocytes. The dense packing of these mononuclear cells includes a high nucleus:cytoplasm ratio that gives a dense basophilic/purple staining under H and E staining conditions.

DISCUSSION

We describe the novel synthesis of a small molecule NHS ester that confers both ^{18}F PET and NIRF visibility onto targeting ligands bearing free amines. Heterobifunctional adapters could easily convert the selectivity toward other reactive groups such as thiols. Because the ^{18}F is appended to the cyanine dye, only one attachment site on the targeting ligand is required. If standard NIRF and PET labels were independently affixed (*4, 7*), at least two chemically reactive yet biologically tolerant sites on the ligand would be required. Unless regioselectivity could be tightly controlled, greater combinatorial complexity of products could result, because each site could remain unmodified or receive a NIRF or PET label. Homogeneous labeling happens not to be essential for Lymphoseek, which already contains a statistical distribution of amines, but Lymphoseek had the advantages of large-scale availability and extensive preclinical and clinical characterization. PET/NIRF-labeled Lymphoseek **3** retains the desired pharmaceutical properties of [^{99m}Tc]Lymphoseek: rapid 1 h sentinel node targeting, low level of distal lymph node accumulation, and sentinel node extraction values (1 nmol dose, 87 ± 7%; 11 nmol

dose, 74 ± 7%) that compare very well to [^{99m}Tc]Lymphoseek extraction ratios, 90 ± 10% in rabbit popliteal SLN (*31, 32*).

PET rapidly and noninvasively quantitates picomole amounts of **1** through deep tissue. An example of the superior tomographic resolution conveyed by ^{18}F PET in Figure 3A is included as an .mpg file (Supporting Information). Notably, this high-resolution projection was generated from a 20 min scan on a live mouse using only 33 μCi of activity. PET is more reliable than NIRF for imaging through deep tissue. This point is illustrated by comparing the skin-on NIRF image (Figure 2Ai) to the skin-off NIRF image (Figure 2Aii). If one were to use Figure 2Ai to evaluate Lymphoseek distribution based on relative NIRF brightness, it would incorrectly appear that the sentinel node (red arrow), buried in muscle and fat, has less Lymphoseek than the lumbar node (blue arrow), which sits next to the spine near the surface of the mouse. Following mouse sacrifice followed by skin removal (Figure 2Aii), we see that the opposite is true and that the NIRF signal is biased to tissue depth. Note that the lymph nodes seen in Figure 2 Ai would be entirely invisible by NIRF if wild-type, hair-bearing mice were used. PET is superior to NIRF in that it allows for quantitative noninvasive deep tissue three-dimensional imaging. Both the live mouse PET images shown in Figure 3 and the .mpg file included as Supporting Information illustrate this. Additional advances in PET imaging may include better CT attenuation algorithms for higher-resolution images and real-time PET reconstruction to guide surgery. If a PET scanner is not available, standard scintigraphic devices can still be used to register the positron-generated γ-rays (*42*−*44*). Consistent with previous studies of ^{18}F-labeled aryltrifluoroborates, no signal is observed in bone structure (Figures 3A and 4), demonstrating the in vivo stability of the aryl trifluoroborate to solvolysis and release of free ^{18}F (*22, 23, 45*).

The stable NIRF component on **1** also allows for NIRF-guided surgery as well as fluorescent histology long after radiotracer decay. Histological resolution (Figure 3D) and the imaging of lymph tracks (Figure 2Bi−iii) are possible only by NIRF, as these structures fall below the spatial detection limits of PET. The heterogeneous foci seen in NIRF histology (Figure 3D) identify the most probable places to find micrometastatic disease in the SLN (*46*), and their fluorescence might reduce the error in pathological evaluations. The heterogeneous distribution of **3** also suggests that only a fraction of the SLN actually filters the afferent lymph channel draining the foot. Both a 1 nmol injection of pure [^{18}F]Lymphoseek **3** and an 11 nmol injection of **3** diluted with unlabeled Lymphoseek are useful in highlighting sentinel popliteal nodes. Our use of a diluted 11 nmol injection may seem superfluous as it requires an extra step in preparation and is slightly inferior to the 1 nmol injection in terms of unwanted flow-through to distal lymph nodes (Table 1). However, the fact that the lymph node mannose receptor binding of **3** can be diluted with unlabeled Lymphoseek such that distal node flow-through is increased serves to illustrate an important trait of the dual probe, that the conjugation of targets to NHS ester **1** does not alter its target's desired diagnostic properties, in this case Lymphoseek's mannose receptor-specific targeting properties.

This PET/NIRF version of Lymphoseek **3** may improve sentinel node biopsy, because a single injection would replace the required multiple-injection combination (*47, 48*) of a radiotracer, such as [^{99m}Tc]Lymphoseek or [^{99m}Tc]sulfur colloid, with a nonspecific optical excision aid such as isosulfan blue dye. Attachment of both the positron emitter and fluorophore to a single molecularly targeted agent diminishes the risk of flow-through to distal lymph nodes and ensures perfect coregistration of the two signals, allowing PET and NIRF to complement each other. PET images would noninvasively identify sentinel nodes that drain a tumor and aid in preoperative planning. During surgery, Geiger counting of the γ-rays could help locate deeply buried nodes. Once they were exposed, higher-resolution real-time NIRF imaging would guide precision resection, including lymph tracks as well as nodes. A postoperative PET scan could confirm whether removal was complete, and NIRF would aid histological identification of metastases within the resected tissue. Successful application of PET/NIRF NHS ester **1** to a well-established, clinically interesting system suggests extension to other medically relevant targets. In previous combinations of PET and NIRF, the positron emitter and fluorophore were independently attached (*4, 7*), whereas **1** combines these capabilities in a single, versatile small molecule only slightly larger than the usual commercially available NIRF labels. It is essential that ^{18}F is incorporated into fluoroborates under mild conditions such as a weakly acidic methanol/water solution at 40 °C, because heptamethine cyanine dyes would not survive high-temperature reaction with anhydrous nucleophilic fluoride as required for traditional ^{18}F chemistries such as fluorobenzyl labeling. Despite scope for further optimization, formation of aryl fluoborate from F^- satisfies many of the criteria for "click chemistry", modularity, high yield, no offensive byproducts, mild aqueous reaction conditions, orthogonality to other functional groups, and simple product isolation (*49*). Although the B−F bond is not as chemically stable as the usual C−F bonds, appropriately substituted aryl fluoborates are stable enough that hydrolysis is negligible within the radioactive half-life of ^{18}F. Our new chemistry should facilitate the multimodality labeling of peptides, proteins, and polysaccharides, medically relevant ligands previously difficult or impossible to label by previous methods.

ACKNOWLEDGMENT

We thank Jacqueline Corbeil for excellent technical assistance with PET, CT, and NIRF imaging studies and Larry Gross for his assistance in obtaining high-resolution mass spectrometry data. This work is supported by the Howard Hughes Medical Institute (HHMI) and Grant W81XWH-05-1-0183 from the Department of Defense Breast Cancer Research Program. R.T. is supported by a Canadian Institute of Health Research (CIHR) Post-Doctoral Fellowship (MFE 83832).

Supporting Information Available: PET/CT video; PET/CT reconstructed data accessible with amide 0.9.1 (http://amide.sourceforge.net); in vivo and synthetic experimental procedures; additional multimodality PET/CT/NIRF data; fluorophore absorption, excitation, and emission spectra; Lymphoseek certificate of analysis; and Lymphoseek in vivo stability and saturation assays. This material is available free of charge via the Internet at http://pubs.acs.org.

LITERATURE CITED

(1) Tsien, R. Y. (2003) Imagining imaging's future. *Nat. Rev. Mol. Cell Biol. 9*, s16–s21.

(2) Bhushan, K. R., Mistra, P., Liu, F., Mathur, S., Lenkinski, R. E., and Frangioni, J. V. (2008) Detection of breast cancer microcalcifications using a dual-modality SPECT/NIR fluorescent probe. *J. Am. Chem. Soc. 130*, 17648–17649.

(3) Pascu, S. I., Waghorn, P. A., Conry, T. D., Betts, H. M., Dilworth, J. R., Churchill, G. C., Pokrovska, T., Christlieb, M., Aigbirhio, F. I., and Warren, J. E. (2007) Designing Zn(II) and Cu(II) derivatives as probes for in vitro fluorescence imaging. *Dalton Trans.,* 4988–4997.

(4) Edwards, W. B., Xu, B., Akers, W., Cheney, P. P., Liang, K., Rogers, B. E., Anderson, C. J., and Achilefu, S. (2008) Agonist-antagonist dilemma in molecular imaging: Evaluation of a monomolecular multimodal imaging agent for the somatostatin receptor. *Bioconjugate Chem. 19*, 192–200.

(5) Duconge, F., Pons, T., Pestourie, C., Herin, L., Theze, B., Gombert, K., Mahler, B., Hinnen, F., Kuhnast, B., Dolle, F., Dubertret, B., and Tavitian, B. (2008) Fluorine-18-labeled phospholipid quantum dot micelles for in vivo multimodal imaging from whole body to cellular scales. *Bioconjugate Chem. 19*, 1921–1926.

(6) Devaraj, N. K., Keliher, E. J., Thurber, G. M., Nahrendorf, M., and Weissleder, R. (2009) F-18 Labeled Nanoparticles for in Vivo PET-CT Imaging. *Bioconjugate Chem. 20*, 397–401.

(7) Kimura, R., Miao, Z., Cheng, Z., Gambhir, S., and Cochran, J. (2010) A Dual-Labeled Knottin Peptide for PET and Near-Infrared Fluorescence Imaging of Integrin Expression in Living Subjects. *Bioconjugate Chem. 21*, 436–444.

(8) Wu, A. M., Yazaki, P. J., Tsai, S. W., Nguyen, K., Anderson, A. L., McCarthy, D. W., Welch, M. J., Shively, J. E., Williams, L. E., Raubitschek, A. A., Wong, J. Y. C., Toyokuni, T., Phelps, M. E., and Gambhir, S. S. (2000) High-resolution microPET imaging of carcino-embryonic antigen-positive xenografts by using a copper-64-labeled engineered antibody fragment. *Proc. Natl. Acad. Sci. U.S.A. 97*, 8495–8500.

(9) Dimitrakopoulou-Strauss, A., Hohenberger, P., Haberkorn, U., Macke, H. R., Eisenhut, M., and Strauss, L. G. (2007) ^{68}Ga-labeled bombesin studies in patients with gastrointestinal stromal tumors: Comparison with ^{18}F-FDG. *J. Nucl. Med. 48*, 1245–1250.

(10) Meyer, G. J., Macke, H., Schuhmacher, J., Knapp, W. H., and Hofmann, M. (2004) ^{68}Ga-labelled DOTA-derivatised peptide ligands. *Eur. J. Nucl. Med. Mol. Imaging 31*, 1097–1104.

(11) Abbas, K., Kozempel, J., Bonardi, M., Groppi, F., Alfarano, A., Holzwarth, U., Simonelli, F., Hofman, H., Horstmann, W., Menapace, E., Leseticky, L., and Gibson, N. (2006) Cyclotron production of Cu-64 by deuteron irradiation of Zn-64. *Appl. Radiat. Isot. 64*, 1001–1005.

(12) Boswell, C. A., Sun, X. K., Niu, W. J., Weisman, G. R., Wong, E. H., Rheingold, A. L., and Anderson, C. J. (2004) Comparative in vivo stability of copper-64-labeled cross-bridged and conventional tetraazamacrocyclic complexes. *J. Med. Chem. 47*, 1465–1474.

(13) Olasz, E. B., Lang, L., Seidel, J., Green, M. V., Eckelman, W. C., and Katz, S. I. (2002) Fluorine-18 labeled mouse bone marrow-derived dendritic cells can be detected in vivo by high resolution projection imaging. *J. Immunol. Methods 260*, 137–148.

(14) Kuhnast, B., de Bruin, A., Hinnen, F., Tavitian, B., and Dolle, F. (2004) Design and synthesis of a new [F-18]fluoropyridine-based haloacetamide reagent for the labeling of oligonucleotides: 2-Bromo-N-[3-(2-[F-18]fluoropyridin-3-yloxy)propyl]acetamide. *Bioconjugate Chem. 15*, 617–627.

(15) Ross, T. L., Ermert, J., Hocke, C., and Coenen, H. H. (2007) Nucleophilic F-18-fluorination of heteroaromatic iodonium salts with no-carrier-added [F-18]fluoride. *J. Am. Chem. Soc. 129*, 8018–8025.

(16) Flavell, R. R., Kothari, P., Bar-Dagan, M., Synan, M., Vallabhajosula, S., Friedman, J. M., Muir, T. W., and Ceccarini, G. (2008) Site-specific F-18-labeling of the protein hormone leptin using a general two-step ligation procedure. *J. Am. Chem. Soc. 130*, 9106–9112.

(17) Glaser, M., and Arstad, E. (2007) "Click labeling" with 2-[F-18]fluoroethylazide for positron emission tomography. *Bioconjugate Chem. 18*, 989–993.

(18) Schirrmacher, R., Bradtmoller, G., Schirrmacher, E., Thews, O., Tillmanns, J., Siessmeier, T., Buchholz, H. G., Bartenstein, P., Wangler, B., Niemeyer, C. M., and Jurkschat, K. (2006) ^{18}F-labeling of peptides by means of an organosilicon-based fluoride acceptor. *Angew. Chem., Int. Ed. 45*, 6047–6050.

(19) Hohne, A., Mu, L., Honer, M., Schubiger, P. A., Ametamey, S. M., Graham, K., Stellfeld, T., Borkowski, S., Berndorff, D., Klar, U., Voigtmann, U., Cyr, J. E., Friebe, M., Dinkelborg, L., and Srinivasan, A. (2008) Synthesis, ^{18}F-labeling, and in vitro and in vivo studies of bombesin peptides modified with silicon-based building blocks. *Bioconjugate Chem. 19*, 1871–1879.

(20) Mu, L., Hohne, A., Schubiger, P. A., Ametamey, S. M., Graham, K., Cyr, J. E., Dinkelborg, L., Stellfeld, T., Srinivasan, A., Voigtmann, U., and Klar, U. (2008) Silicon-based building blocks for one-step ^{18}F-radiolabeling of peptides for PET imaging. *Angew. Chem., Int. Ed. 47*, 4922–4925.

(21) Schirrmacher, E., Wangler, B., Cypryk, M., Bradtmoller, G., Schafer, M., Eisenhut, M., Jurkschat, K., and Schirrmacher, R. (2007) Synthesis of p-(di-tert-butyl[^{18}F]fluorosilyl)benzaldehyde ([^{18}F]SiFA-A) with high specific activity by isotopic exchange: A convenient labeling synthon for the ^{18}F-labeling of N-aminooxy derivatized peptides. *Bioconjugate Chem. 18*, 2085–2089.

(22) Ting, R., Harwig, C. W., Lo, J., Li, Y., Adam, M. J., Ruth, T. J., and Perrin, D. M. (2008) Substituent effects on aryltrifluoroborate solvolysis in water: Implications for Suzuki-Miyaura coupling and the design of stable F-18-labeled aryltrifluoroborates for use in PET imaging. *J. Org. Chem. 73*, 4662–4670.

(23) Ting, R., Lo, J., Adam, M. J., Ruth, T. J., and Perrin, D. M. (2008) Capturing aqueous [F-18]-fluoride with an arylboronic ester for PET: Synthesis and aqueous stability of a fluorescent [F-18]-labeled aryltrifluoroborate. *J. Fluorine Chem. 129*, 349–358.

(24) Ting, R., Adam, M. J., Ruth, T. J., and Perrin, D. M. (2005) Arylfluoroborates and alkylfluorosilicates as potential PET imaging agents: High-yielding aqueous biomolecular F-18-labeling. *J. Am. Chem. Soc. 127*, 13094–13095.

(25) Ting, R., Harwig, C., auf dem Keller, U., McCormick, S., Austin, P., Overall, C. M., Adam, M. J., Ruth, T. J., and Perrin, D. M. (2008) Toward [F-18]-labeled aryltrifluoroborate radiotracers: In vivo positron emission tomography imaging of stable aryltrifluoroborate clearance in mice. *J. Am. Chem. Soc. 130*, 12045–12055.

(26) Valk, P. E., Bailey, D. L., Townsend, D. W., and Maisey, M. N. (2003) *Positron Emission Tomography: Basic Science and Clinical Practice*, Springer-Verlag, London.

(27) Hirsch, J. I., Tisnado, J., Cho, S. R., and Beachley, M. C. (1982) Use of Isosulfan Blue for Identification of Lymphatic Vessels: Experimental and Clinical Evaluation. *Am. J. Roentgenol. Radium Ther. 139*, 1061–1064.

(28) Mariani, G., Gipponi, M., Moresco, L., Villa, G., Bartolomei, M., Mazzarol, G., Bagnara, M. C., Romanini, A., Cafiero, F., Paganelli, G., and Strauss, H. W. (2002) Radioguided sentinel lymph node biopsy in malignant cutaneous melanoma. *J. Nucl. Med. 43*, 811–827.

(29) Mariani, G., Moresco, L., Viale, G., Villa, G., Bagnasco, M., Canavese, G., Buscombe, J., Strauss, H. W., and Paganelli, G. (2001) Radioguided sentinel lymph node biopsy in breast cancer surgery. *J. Nucl. Med. 42*, 1198–1215.

(30) Weaver, D. L., Krag, D. N., Ashikaga, T., Harlow, S. P., and O'Connell, M. (2000) Pathologic analysis of sentinel and nonsentinel lymph nodes in breast carcinoma: A multicenter study. *Cancer 88*, 1099–1107.

(31) Vera, D. R., Wisner, E. R., and Stadalnik, R. C. (1997) Sentinel node imaging via a nonparticulate receptor-binding radiotracer. *J. Nucl. Med. 38*, 530–535.

(32) Vera, D. R., Wallace, A. M., Hoh, C. K., and Mattrey, R. F. (2001) A synthetic macromolecule for sentinel node detection: Tc-99m-DTPA-mannosyl-dextran. *J. Nucl. Med. 42*, 951–959.

(33) Hoh, C. K., Wallace, A. M., and Vera, D. R. (2003) Preclinical studies of [Tc-99m]DTPA-mannosyl-dextran. *Nucl. Med. Biol. 30*, 457–464.

(34) Vera, D. R., Wallace, A. M., and Hoh, C. K. (2001) [Tc-99m]MAG_3-mannosyl-dextran: A receptor-binding radiopharmaceutical for sentinel node detection. *Nucl. Med. Biol. 28*, 493–498.

(35) Schoder, H., Glass, E. C., Pecking, A. P., Harness, J. K., Wallace, A. M., Hirnle, P., Alberini, J. L., Vilain, D., Larson, S. M., Hoh, C. K., and Vera, D. R. (2006) Molecular targeting of the lymphovascular system for imaging and therapy. *Cancer Metastasis Rev. 25*, 185–201.

(36) Dubois, M., Gilles, K. A., Hamilton, J. K., Rebers, P. A., and Smith, F. (1956) Colorimetric Method for Determination of Sugars and Related Substances. *Anal. Chem. 28*, 350–356.
(37) Hall, D. J., Sunar, U., Farshchi-Heydari, S., and Han, S. H. (2009) In vivo simultaneous monitoring of two fluorophores with lifetime contrast using a full-field time domain system. *Appl. Opt. 48*, D74–D78.
(38) Fox, I. J., and Wood, E. H. (1960) Indocyanine Green: Physical and Physiologic Properties. *Proc. Staff Meet. Mayo Clin. 35*, 732–744.
(39) Fox, I. J., Brooker, L. G. S., Heseltine, D. W., Essex, H. E., and Wood, E. H. (1956) New Dyes for Continuous Recording of Dilution Curves in Whole Blood Independent of Variations in Blood Oxygen Saturation. *Am. J. Physiol. 187*, 599.
(40) Lee, H., Mason, J. C., and Achilefu, S. (2006) Heptamethine cyanine dyes with a robust C-C bond at the central position of the chromophore. *J. Org. Chem. 71*, 7862–7865.
(41) Limmer, K., and Vera, D. R. Manuscript in preparation.
(42) Bax, J. J., Visser, F. C., van Lingen, A., Huitink, J. M., Kamp, O., van Leeuwen, G. R., Visser, G. W., Teule, G. J., and Visser, C. A. (1993) Feasibility of assessing regional myocardial uptake of ^{18}F-fluorodeoxyglucose using single photon emission computed tomography. *Eur. Heart J. 14*, 1675–1682.
(43) Knesaurek, K., and Machac, J. (2006) Comparison of ^{18}F SPECT with PET in myocardial imaging: A realistic thoraxcardiac phantom study. *BMC Nucl. Med. 6*, 5.
(44) Leichner, P. K., Morgan, H. T., Holdeman, K. P., Harrison, K. A., Valentino, F., Lexa, R., Kelly, R. F., Hawkins, W. G., and Dalrymple, G. V. (1995) SPECT imaging of fluorine-18. *J. Nucl. Med. 36*, 1472–1475.
(45) Bohn, P., Deyine, A., Azzouz, R., Bailly, L., Fiol-Petit, C., Bischoff, L., Fruit, C., Marsais, F., and Vera, P. (2009) Design of silicon-based misonidazole analogues and ^{18}F-radiolabelling. *Nucl. Med. Biol. 36*, 895–905.
(46) Haigh, P. I., Lucci, A., Turner, R. R., Bostick, P. J., Krasne, D. L., Stern, S. L., and Morton, D. L. (2001) Carbon dye histologically confirms the identity of sentinel lymph nodes in cutaneous melanoma. *Cancer 92*, 535–541.
(47) Chen, S. L., Iddings, D. M., Scheri, R. P., and Bilchik, A. J. (2006) Lymphatic mapping and sentinel node analysis: Current concepts and applications. *Ca—Cancer J. Clin. 56*, 292–309 (quiz 316−317).
(48) Edwards, M. J., Martin, K. D., and McMasters, K. M. (1999) Lymphatic mapping and sentinel lymph node biopsy in the staging of melanoma. *Surg. Oncol.,* 51–57.
(49) Kolb, H. C., Finn, M. G., and Sharpless, K. B. (2001) Click chemistry: Diverse chemical function from a few good reactions. *Angew. Chem., Int. Ed. 40*, 2004–2021.

BC1001328